Paleogene propagation of the southern Pyrenean thrust wedge revealed by finite strain analysis in frontal thrust sheets: Implications for mountain building

Huyghe, D.; Mouthereau, F.; Castelltort, Sébastien; Filleaudeau, P.Y.; Emmanuel, L.

How to cite

HUYGHE, D. et al. Paleogene propagation of the southern Pyrenean thrust wedge revealed by finite strain analysis in frontal thrust sheets: Implications for mountain building. In: Earth and planetary science letters, 2009, vol. 288, n° 3-4, p. 421–433. doi: 10.1016/j.epsl.2009.10.002

This publication URL: https://archive-ouverte.unige.ch/unige:20395

Publication DOI: 10.1016/j.epsl.2009.10.002

Earth and Planetary Science Letters 288 (2009) 421–433

Contents lists available at ScienceDirect

Earth and Planetary Science Letters

journal homepage: www.elsevier.com/locate/epsl

Paleogene propagation of the southern Pyrenean thrust wedge revealed by finite strain analysis in frontal thrust sheets: Implications for mountain building

D. Huyghe [a,*], F. Mouthereau [a,c], S. Castelltort [b], P.Y. Filleaudeau [a], L. Emmanuel [a]

[a] Institut des Sciences de la Terre et de l'Environnement de Paris, Université Pierre et Marie Curie – Paris 6, Paris, France
[b] Geological Institute, Earth Surface Dynamics, ETH, Zürich, Switzerland
[c] Centre de Recherches Pétrographiques et Géochimiques, Vandœuvre-lès-Nancy, France

ARTICLE INFO

Article history:
Received 1 April 2009
Received in revised form 3 October 2009
Accepted 6 October 2009
Available online 5 November 2009

Editor: T.M. Harrison

Keywords:
Pyrenees
strain
kinematics
Paleogene
mountain building
mass balance

ABSTRACT

To better evaluate the sequence of shortening and estimate shortening rates associated with the propagation of the southern Pyrenean front, we propose an original approach based on the reconstruction of finite displacement and finite vertical-axis rotations. This study is based on the quantitative analysis of published datasets including balanced cross-sections, paleomagnetic and thermochronologic data. We distinguish three main episodes of shortening between 41 and 37 Ma, 37 and 30 Ma and between 30 and 16 Ma. They are associated with a decrease of accretionary rates from ~3 km/Ma to 0.39 ± 0.27 km/Ma on the pro-wedge side of the Pyrenean orogenic wedge. Based on the comparison between frontal accretionary flux and outcoming fluxes in the Axial Zone of the Pyrenees, we show that the period ranging from 37 to 30 Ma recorded a remarkable increase in erosion that is not compensated by accretion in the wedge. In the context of the overall decrease in the Iberia/Eurasia plate convergence, we suggest that the main cause of the acceleration of erosion on top of the growing Pyrenean orogen is related to climate changes that occurred at the Eocene–Oligocene boundary.

1. Introduction

Among ancient fold-and-thrust belts, the southern Pyrenean fold-and-thrust belt is one of the most studied because of the remarkable field exposures of syntectonic stratigraphic features allowing for accurate dating of individual thrust sheet activity (Muñoz, 1992; Vergés et al., 1995; Meigs et al., 1996; Teixell, 1996; Meigs and Burbank, 1997; Vergés et al., 2002). These works established that the southern Pyrenean front propagated southwards starting with basin inversion in the Late Cretaceous followed by thin-skinned evolution of the fold-and-thrust belt throughout the Paleogene. The cessation of tectonic activity occurred in the Miocene due to the consumption of Iberia/Eurasia plate convergence. The southward propagation, reflecting the growth of the Pyrenean orogenic wedge, was associated with a contemporaneous lateral propagation of the deformation as outlined by the presence of oblique folds and thrust ramps. The western part of the southern Pyrenean fold-and-thrust offers a remarkable example of the interactions between both N–S and E–W transport of thrust sheets (Figs. 1 and 2). On the eastern boundary of the Jaca piggy-back basin, the Boltaña anticline oriented N–S developed during the Mid-Eocene in relation with the westward propagation of the larger scale Gavarnie–Boltaña unit and acted as a major topographic barrier in the southern Pyrenean foreland basin (Fig. 2). The emplacement of the Gavarnie–Boltaña unit occurred during the Late Lutetian until the Bartonian. It is part of a larger E–W sequence of folding starting from the East, with the Mediano anticline development during the Early–to-Late Lutetian, and propagating to the West with the growth of the "Sierras Exteriores", including the Pico del Aguila anticline, which developed through the Bartonian and until the Early Priabonian (Poblet and Hardy, 1995; Castelltort et al., 2003). These tectonic features, oblique to the regional southward transport direction of thrust sheets, are probably kinematically linked to the southward-propagating thrust ramps. A classical way to explain the coexistence of different fold orientations associated with a single tectonic event is to demonstrate that the oblique features experienced a vertical-axis rotation. Paleomagnetic measurements within the Bartonian succession of the Sierras Exteriores showed that the N–S trending Pico del Aguila anticline recorded a mean clockwise rotation of 21.1° ± 8.8° given data presented in Pueyo et al. (2002). By combining all paleomagnetic constraints available within the Jaca basin, Sierras Exteriores and inner thrust sheets, Oliva-Urcia and Pueyo (2007) consistently proposed a weighted rotation value of the order of 20°. However, because paleomagnetic rotation axes are not mutually independent, the order of rotations makes no difference to the finite rotation measured by paleomagnetic data. The knowledge of the true

* Corresponding author. Institut des Sciences de la Terre et de l'Environnement de Paris, Université Pierre et Marie Curie, T. 55–56, E5, Box 116, 75252 Paris Cedex 05, France. Tel.: +33 144274995; fax: +33 144273831.
E-mail address: damien.huyghe@upmc.fr (D. Huyghe).

0012-821X/$ – see front matter © 2009 Elsevier B.V. All rights reserved.
doi:10.1016/j.epsl.2009.10.002

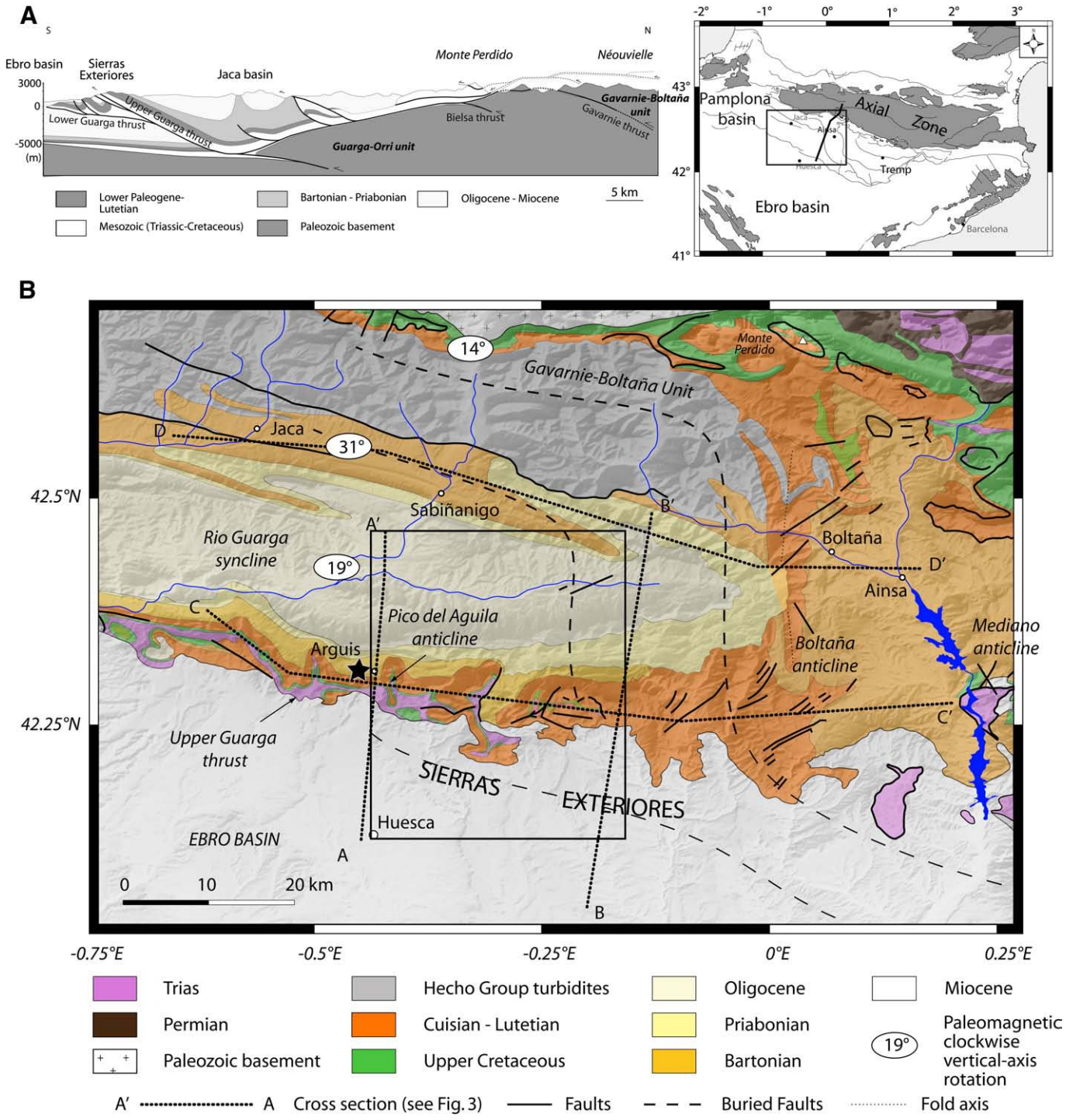

Fig. 1. A) Regional cross-section of the studied area in the framework of the Pyrenean collision. B) Geological map of the western part of the South Pyrenean fold-thrust belt with location of the balanced cross-sections used to calculate the displacement field. The grey quadrangle defines the area where the distribution of shortening in the E–W and N–S direction is constrained by cross-sections AA′, BB′, CC′ and DD′ presented in Fig. 3. Values in degrees are paleomagnetic vertical-axis rotations in the northern internal sierras (14°; 8 paleomagnetic data), central Jaca basin and eastern Boltaña anticline (31°; 17 paleomagnetic data) and Sierras Exteriores (19°; 14 paleomagnetic data) after compilation recently published (Oliva-Urcia and Pueyo, 2007). Taken together these data reveal a weighted average clockwise vertical-axis rotation of 22° for the whole studied area. Dashed lines represent buried thrusts and the black star points to the Arguis syncline in which a paleomagnetic study yielded a rotation of 21.1° ± 8.8° within the Bartonian sediments (Pueyo et al., 2002). Note that units in the hangingwall of the Upper Guarga thrust (e.g. Cuisian–Lutetian limestones) are either blanketed by Miocene sedimentation of the Ebro basin to the East or are tectonically overthrusting the Miocene sediments to the West (Trias exposed at the surface).

Fig. 2. Combined E–W and N–S sequence of deformation in the western Pyrenean foreland fold-thrust belt based on information compiled from tectonic–stratigraphic relationships associated with major cover folds and faults (Muñoz, 1992; Vergés et al., 1995; Meigs et al., 1996; Teixell, 1996; Meigs and Burbank, 1997; Pueyo et al., 2002; Vergés et al., 2002) and thermochronometric ages in the hangingwall of major basement thrusts (Morris et al., 1998; Fitzgerald et al., 1999; Sinclair et al., 2005; Gibson et al., 2007). The thick black dashed line outlines the westward and southward migration of the deformation. Question marks point to the lack of stratigraphic constraints on tectonic activity during the Late Eocene–Early Oligocene in our study area. As a consequence, the deformation associated with the Upper Guarga thrust and the Pico del Aguila anticline appears disconnected. Montsech thrust as well as the Cotiella and Peña–Montanesa nappes are mentioned for references to the eastern and central Pyrenees. Black and grey lines are thrusts and folds, respectively.

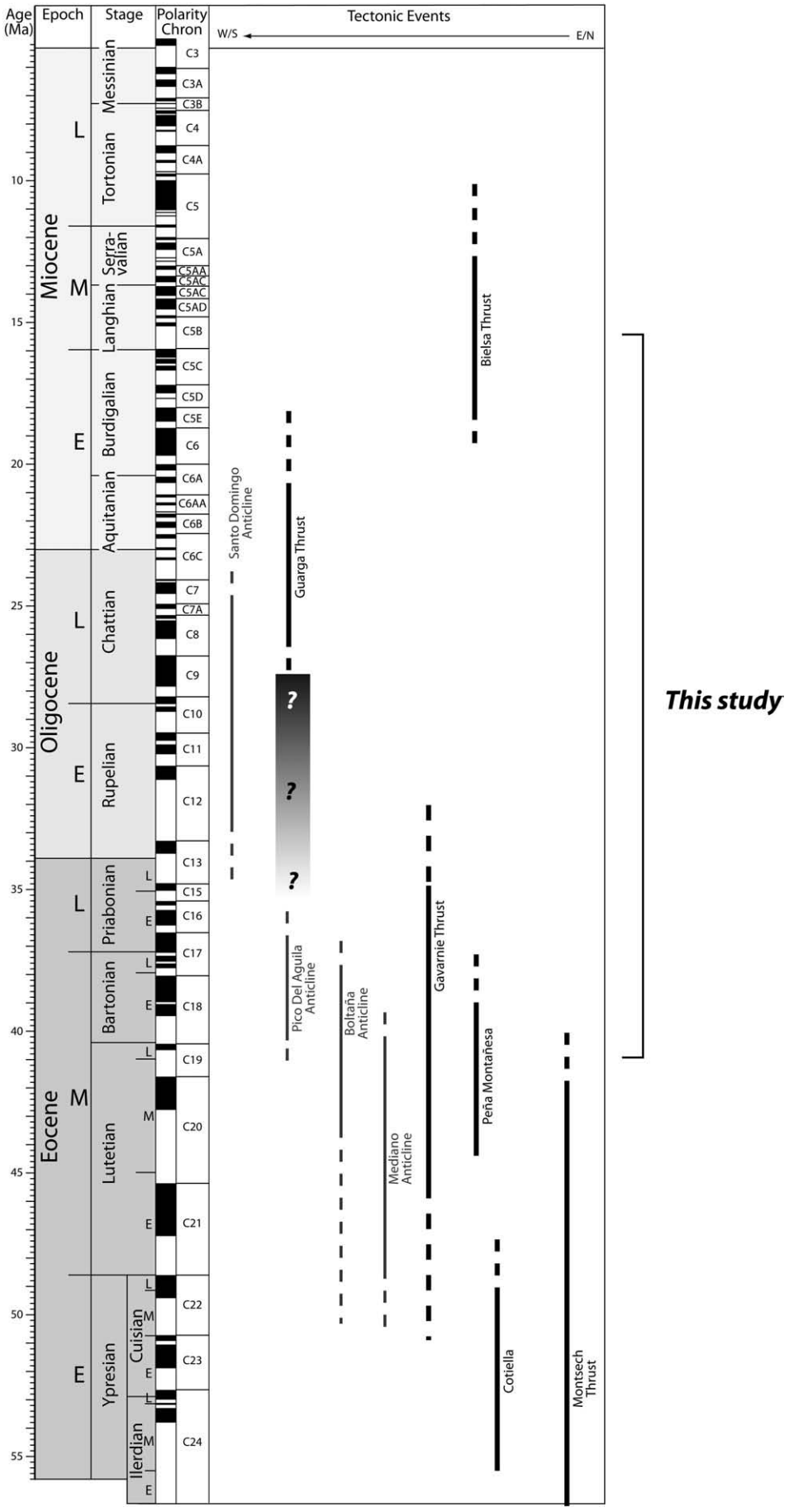
Age (Ma)
Epoch
Stage
Polarity Chron
Tectonic Events
W/S
E/N
Miocene
Oligocene
Eocene
Messinian
Tortonian
Serra-valian
Langhian
Burdigalian
Aquitanian
Chattian
Rupelian
Priabonian
Bartonian
Lutetian
Ypresian
Cuisian
Ilerdian
Santo Domingo Anticline
Guarga Thrust
Bielsa Thrust
Pico Del Aguila Anticline
Boltaña Anticline
Mediano Anticline
Gavarnie Thrust
Peña Montañesa
Cotiella
Montsech Thrust
This study

sequence of rotation and shortening should therefore take into account other independent constraints.

By the Late Oligocene–Early Miocene times, the current structural setting of the Sierras Exteriores was achieved in association with the southward displacement along the Guarga thrust ramp (hereinafter called Upper Guarga thrust). This led to the exposure of the Mesozoic limestones and the thick overlying syn-orogenic Cenozoic cover, including the well-known Lutetian limestones of the Guara Formation. The timing is constrained by the presence of cobbles of Guara limestones within the Late Oligocene–Early Miocene piedmont alluvial fans of the Upper Guarga thrust ramp (Hirst and Nichols, 1986). One can presume that the pre-Miocene component of N–S displacement might have been significant along the thrust ramp in order to raise the Guara limestones to the surface and erode a significant part of the Cenozoic strata. Unfortunately the sequence of deformation associated with the early kinematics of the Guarga thrust sheets is still unconstrained due to the lack of syn-thrusting sediments.

To summarize, the Bartonian deformation observed at the southern Pyrenean thrust front are still not clearly associated with quantitative estimates of E–W and N–S displacements. Furthermore, the kinematics of the main frontal thrust during the Paleogene is still largely unknown due to the absence of preserved syntectonic strata. These are major issues to address in order to better constrain the timing of mountain building in the Pyrenees and understand better the evolution of orogenic fluxes. In this paper, we adopt an original approach based on the reconstruction of the finite displacement field from which the finite strain field can be deduced. We focus particularly on the comparison between calculated rigid vertical-axis rotations related to E–W and N–S differential shortening and observed paleomagnetic rotations. By restoring, in successive steps, the displacements accumulated across the frontal thrusts and folds, we determine a possible scenario for the origin of the observed paleomagnetic rotations. The obtained shortening history at the belt front is then used as additional constraints on the growth of the Pyrenean wedge during the Paleogene. Finally, we put together these results with thermochronometric ages in order to examine the evolution of orogenic fluxes.

2. Geological background

2.1. Structural features

The western Pyrenean foreland fold-and-thrust belt (Fig. 1) to the West of the Boltaña anticline involves from North to South: 1) the Jaca basin, a transported and folded Paleogene foredeep; 2) Mesozoic-to-Paleogene series forming a rough relief called the “Sierras Exteriores” in the hangingwall of the Upper Guarga thrust; 3) Paleogene-to-Neogene continental deposits at the northern edge of the Ebro basin, which is the current foreland basin of the southern Pyrenees.

The sedimentary cover in the hangingwall of the Upper Guarga thrust (Fig. 1) includes an evaporitic Trias overlain by a condensed succession of upper Cretaceous shelfal limestones (Millán et al., 1994). Above this Mesozoic succession, the syn-collisional deposits begin with Lutetian limestones of the Guara formation, which form the backbone of the Sierras Exteriores. They are covered by syn-orogenic siliciclastics shallowing upwards from marine deltaics in the Bartonian to fluvial sequences in the Priabonian. Northwards, into the Guarga syncline, this succession grades upwards into Late Oligocene–Early Miocene continental conglomerates.

Four cross-sections were established using published geological sections (Millán Garrido, 1996; Fernàndez et al., 2004) and a few additional mapping (Fig. 3). Two of them (sections AA′ and BB′) cut approximately N–S through the Guarga syncline and the Guarga thrust sheets in order to best provide constraints on the N–S transport. Two new sections are oblique, approximately orogen-parallel, in order to constrain the E–W transport (sections CC′ and DD′). Taken together, these four sections form a composite array of which the complete finite displacement field can be derived. Basically, sections AA′ and BB′ reveal that the Guarga thrust sheet resulted from both thin-skinned deformation on top of the Triassic evaporitic décollement and thick-skinned deformation as the upper décollement plunges, northwards, into a deep-seated basement ramp at the origin of the rio Guarga syncline in the sediment cover (Fig. 3).

2.2. Constraints on the E–W and N–S sequence of deformation

Fig. 2 shows a synthesis of E–W and N–S sequence of deformation in the western Pyrenean foreland fold-thrust belt. For instance, map-scale unconformities as well as magnetic stratigraphy of syntectonic strata (e.g. Holl and Anastasio, 1993) established that the Mediano anticline was active during the Lutetian (Fig. 2). Westward, the Boltaña anticline, which is part of the larger Boltaña–Gavarnie unit likely developed during the Middle Lutetian until the Early Priabonian (Puigdefàbregas and Souquet, 1986). This is consistent with thermochronometric constraints indicating a Late Eocene age for the exhumation in the hangingwall of the Gavarnie basement thrust (e.g. Sinclair et al., 2005; Jolivet et al., 2007). The Sierras Exteriores are characterized by a series of anticlines with fold axes trending N–S on average. The analysis of syntectonic strata associated with these folds has clearly emphasized a Bartonian age for folding (Millán et al., 1994; Poblet and Hardy, 1995; Hogan and Burbank, 1996; Pueyo et al., 2002).

The emergent Upper Guarga thrust ramp is at the origin of the morphological thrust front outlined by the Sierras Exteriores (Fig. 1). Cross-sections reveal that it is an out-of-sequence unit overthrusting lower buried thrust sheets (Fig. 3). The more recent N–S displacement along the Guarga basement thrust interferes with older E–W displacements, which caused the tilting of Oligocene strata in the northern flank of the rio Guarga syncline. Evidence of syntectonic strata of Priabonian age, in the North of the rio Guarga syncline, found in association with E–W trending folds (Hogan and Burbank, 1996; Teixell, 1998) suggest that N–S displacements were significant along the Upper Guarga thrust ramp prior to the Miocene (Fig. 2).

3. Methodology: reconstruction of sequence of deformation using constraints on paleomagnetic rotations

3.1. Finite displacements and rotations

Cross-sections in Fig. 3 show contrasting shortening distribution in the E–W and N–S directions. Assuming no significant deformation out of the studied geological sections such lateral gradients of deformation imply finite shear strains and rotations within the thrust sheets.

In the aim at providing constraints on the finite shortening and finite rotation in the studied area, we have first established the finite displacement field based on the set of four balanced cross-sections presented in Fig. 3. Each section has been restored backwards in its original geometry with respect to the Guara limestones, which are the youngest pre-shortening level that can be considered initially horizontal. This approximation has little consequence on the results since we are interested mainly on the horizontal displacement field. The top of the Guara layer has been digitized every ~1 km for each pair of deformed/restored sections. Differentiating between the final/deformed and the original/restored geometry gives the 2D displacement field along the strike of the studied sections from which the horizontal and vertical components can be obtained (Fig. 4). The same approach has been adopted for each of the four sections.

Assuming a continuous strain field between the studied sections, the horizontal components of the 2D displacement fields were linearly interpolated in a square grid of $1' \times 1'$ whose limits are ($-0.439°$E, $-0.15°$E) and (42.15°N, 42.398°N) for the minimum and maximum longitudes and latitudes, respectively. We finally yield two continuous E–W and N–S velocity vector fields defined respectively by u_x (velocities along x-axis taken positive to the East) and u_y (velocities

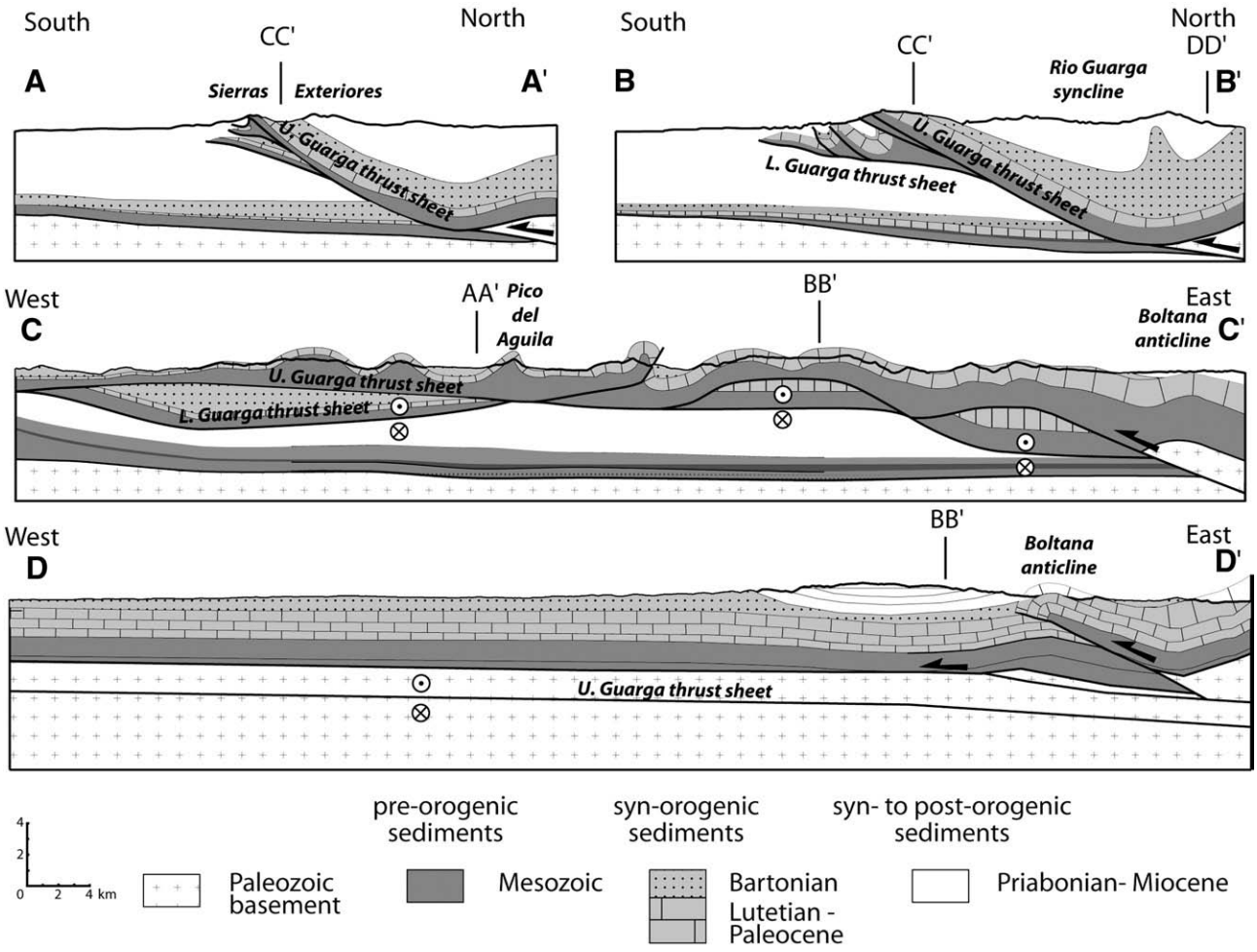

Fig. 3. Cross-sections used in this study (see location in Fig. 1). Sections AA′ and BB′ striking N–S are adapted from Millán Garrido (1996). Sections CC′ and DD′ have been constrained based on surface and subsurface data published in Millán Garrido (1996) and Fernàndez et al. (2004) and map constraints. The superimposition of tectonic units in section DD′ reveals the presence of south-transported thrust sheet imbricated below the main Upper Guarga ramp.

along *y*-axis taken positive to the North). The sum of the two fields gives the complete displacement field $\mathbf{u}=(\mathbf{u}_x, \mathbf{u}_y)$ shown in Fig. 5. Taking spatial derivatives of the components of the displacement give the displacement gradient matrix $\nabla\mathbf{u}$ which is defined by

$$\nabla\mathbf{u} = \begin{pmatrix} \frac{du_x}{dx} & \frac{du_x}{dy} \\ \frac{du_y}{dx} & \frac{du_y}{dx} \end{pmatrix} \quad (1)$$

which could be divided into its symmetric part, the strain tensor $\mathbf{e}$ ($\mathbf{e}_{ij}=\mathbf{e}_{ji}$),

$$\mathbf{e} = \begin{pmatrix} \frac{du_x}{dx} & \frac{1}{2}\left(\frac{du_y}{dx}+\frac{du_x}{dy}\right) \\ \frac{1}{2}\left(\frac{du_x}{dy}+\frac{du_y}{dx}\right) & \frac{du_y}{dy} \end{pmatrix} \quad (2)$$

and its antisymmetric part, the rotation tensor $\mathbf{\Omega}$ ($\mathbf{\Omega}_{ij}=-\mathbf{\Omega}_{ji}$),

$$\mathbf{\Omega} = \begin{pmatrix} 0 & -\frac{1}{2}\left(\frac{du_y}{dx}-\frac{du_x}{dy}\right) \\ -\frac{1}{2}\left(\frac{du_x}{dy}-\frac{du_y}{dx}\right) & 0 \end{pmatrix} \quad (3)$$

Both strain and rotation tensors, at any points of the grid, have three unknowns. They are solved by taking the components of the finite displacement vectors at 3 adjacent vertices. The eigenvalues and eigenvectors of $\mathbf{e}$ and $\mathbf{\Omega}$ matrices provide magnitudes and orientations of the principal strain axes and rigid rotations (see files given as supplementary material).

3.2. Cautions and sources of errors on measured and predicted finite rotations and strains

A large collection of paleomagnetic data is currently available in our studied area of the southern Pyrenees (Dinarès et al., 1992; Pueyo et al., 2002; Oliva-Urcia and Pueyo, 2007). These data provide constraints on finite rotations about vertical axis in southern Pyrenean thrust sheets that can therefore be compared to the finite rotations predicted by our kinematic model.

However, we should be cautious with the interpretation of paleomagnetic rotations because they can be the sum of any number of finite rotations about different axes (e.g. McCaig and McClelland, 1992). For instance, in case of paleomagnetic studies carried out in folds originated at oblique ramps, i.e. oblique to the transport directions (Mouthereau et al., 1999), the restored orientation of a paleomagnetic vector may produce a spurious vertical-axis rotation related to the interaction of more than one horizontal axes of tilting, with different orientations and magnitudes (Pueyo et al., 2003). Spurious vertical-axis rotation can also occur in case the bedding

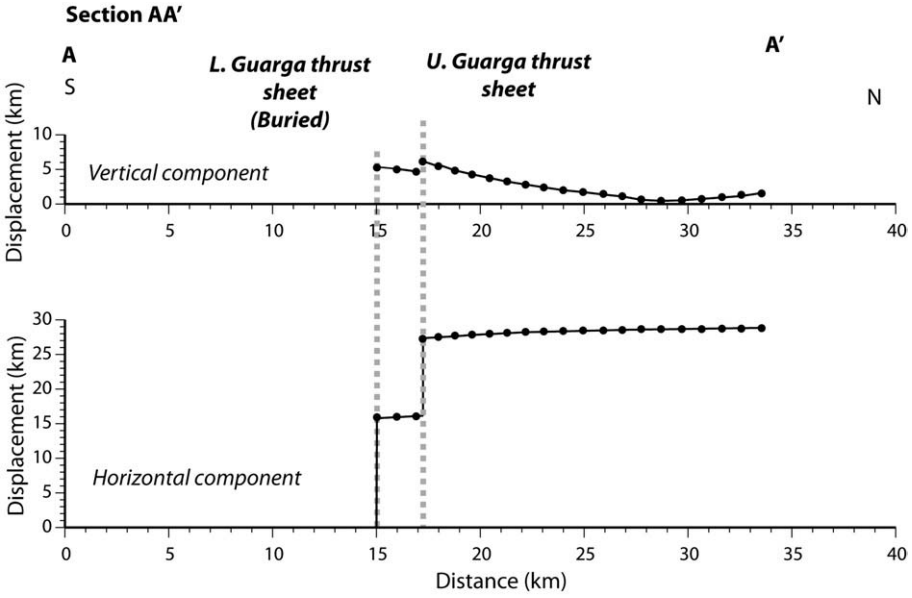

Fig. 4. Example of the decomposition of both horizontal and vertical components of displacement obtained along section AA′ (Fig. 3). Black dots represent sampled points located in their present position in section AA′ (not restored). Displacements are obtained by differentiating between current and restored geometry of an initially horizontal reference layer (Guara limestones) from which the different components are calculated. The hangingwall of the Upper Guarga thrust, located at 17.5 km, has been uplifted by ~6 km and shortened by ~27 km with respect to its undeformed foreland position. On the other hand, the Lower Guarga thrust sheet, whose southern tip is located at 15 km, was thrusted by 15 km.

plane has not been titled by a rotation axis oblique to the strike of bedding. The absence of internal deformation (grain-scale tectonic movements) is also a major assumption behind any paleomagnetic reconstruction. As a consequence, in localities where important local deformation has been independently documented, more rotations can occur at local scale but are not necessarily related to the regional shortening gradient.

It is also worth noting that working with large finite deformation theoretically does not permit the use of Eqs. (1)–(3), which are only valid for small strains where the product of the components of $\nabla\mathbf{u}$ is $\ll 1$. However, we favor this solution which has the advantage of being simple and straightforward for calculating strains and rotations despite the loss in accuracy. This is acceptable if the finite deformation history is divided into a series of individual settings recording smaller deformation. Considering the above limitations it is important to remind that the rotations calculated in this study are used in combination with stratigraphic data to yield first order information on the shortening and sequence of deformation, which are the main objectives of this study.

4. Patterns of Bartonian-to-Miocene rotations at the southern Pyrenean thrust front

4.1. E–W and N–S components of finite shortening and rigid rotations

Fig. 5 shows the complete displacement field deduced from the restoration of cross-sections presented in Fig. 3. According to the timing of deformation associated with the N–S-trending folds (Boltaña, Pico del Aguila) the E–W component of deformation was achieved no later than the Bartonian (Fig. 2). Following the same logic, the N–S component is related to the distribution of shortening that terminated during the pre-Priabonian to the early Miocene.

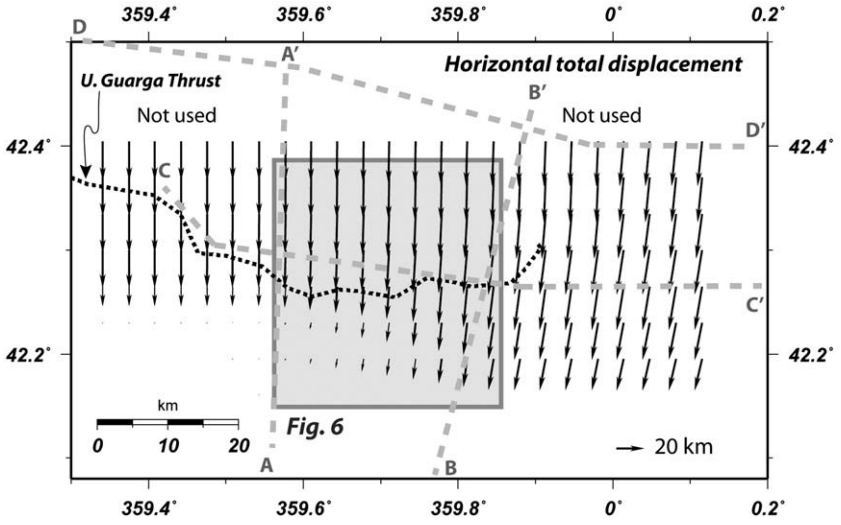

Fig. 5. Finite displacement field (horizontal component) over the whole studied area deduced from linear interpolation of fully restored of N–S (AA′ and BB′ of Fig. 3) and E–W (CC′ and DD′ of Fig. 3) cross-sections represented as grey dashed lines (see also Fig. 1 or 3). The black dashed line represents the trace of the Upper Guarga thrust. We have also depicted portions of the displacement field, which lack of sufficient kinematic information from both E–W and N–S field; they have not been used in this study.

Fig. 6A–C illustrates N–S, E–W and total displacement fields, respectively. Finite rotations caused by the differential shortening in the Lower and Upper Guarga thrust sheets are also plotted. All results are synthesized in Table 1. The N–S displacement field reveals clockwise rotations of 14.2° ± 2.3° with a maximum of 22.3° in the basal thrust unit located in the footwall of the Upper Guarga thrust ramp (Model 1, Fig. 6A and Table 1). These rotations are the result of the shortening distribution observed in the Lower Guarga thrust sheet (Fig. 3). In contrast, the E–W displacement field (Model 2, Fig. 6B) predicts much smaller clockwise rotations of 3.1° ± 0.4° in the hangingwall of the emergent Upper Guarga thrust ramp (Fig. 5B and Table 1). The combination of both N–S and E–W fields gives the total finite displacement field (Model 3, Fig. 6C), which predicts rotations in the footwall of the Upper Guarga thrust up to 22.3° and values of maximum 10.7° in its hangingwall. This latter result reflects the limited lateral gradient of N–S deformation in this unit.

4.2. On the origin of rigid rotations in the Guarga thrust sheets

Model 4 (Fig. 6D) illustrates the displacement field after the restoration of out-of-sequence movement along the Upper Guarga thrust ramp. This was obtained by removing the horizontal gradient of displacement between the lower and upper thrust sheets as briefly illustrated in Fig. 7. The restoration leads to move the hangingwall by 9.5 ± 2.6 km northwards (Table 1). Errors on the mean total displacement are caused by the longitudinal gradient of restored displacements. The new picture of the finite displacement in the hangingwall reproduces a mean rotation of 16.6° ± 1.5° with peak rotations of 20.8° in agreement with observed paleomagnetic rotations (Pueyo et al., 2002; Oliva-Urcia and Pueyo, 2007). This restoration (Model 4, Fig. 6D) has permitted the recovery of the primary clockwise rotation of ~20° which is masked by the secondary counterclockwise rotation associated with out-of-sequence displacement along the Upper Guarga thrust. As indicated in the introduction, the timing of activity along the Upper Guarga thrust ramp is constrained by the occurrence of Late Oligocene–Early Miocene coarse alluvial deposition in the Ebro basin. As a consequence, the rotation and displacement field of Fig. 6D likely predated the Late Oligocene–Early Miocene.

In the following, we seek to determine the displacement field responsible for 20° clockwise rotation achieved during the Bartonian. Since translation does not affect rotations, we have first restored backwards, in the N–S direction, the Lower Guarga unit by the maximum amounts leaving unchanged the rotations reconstructed in the previous step. We obtain a mean displacement of 10 km in the

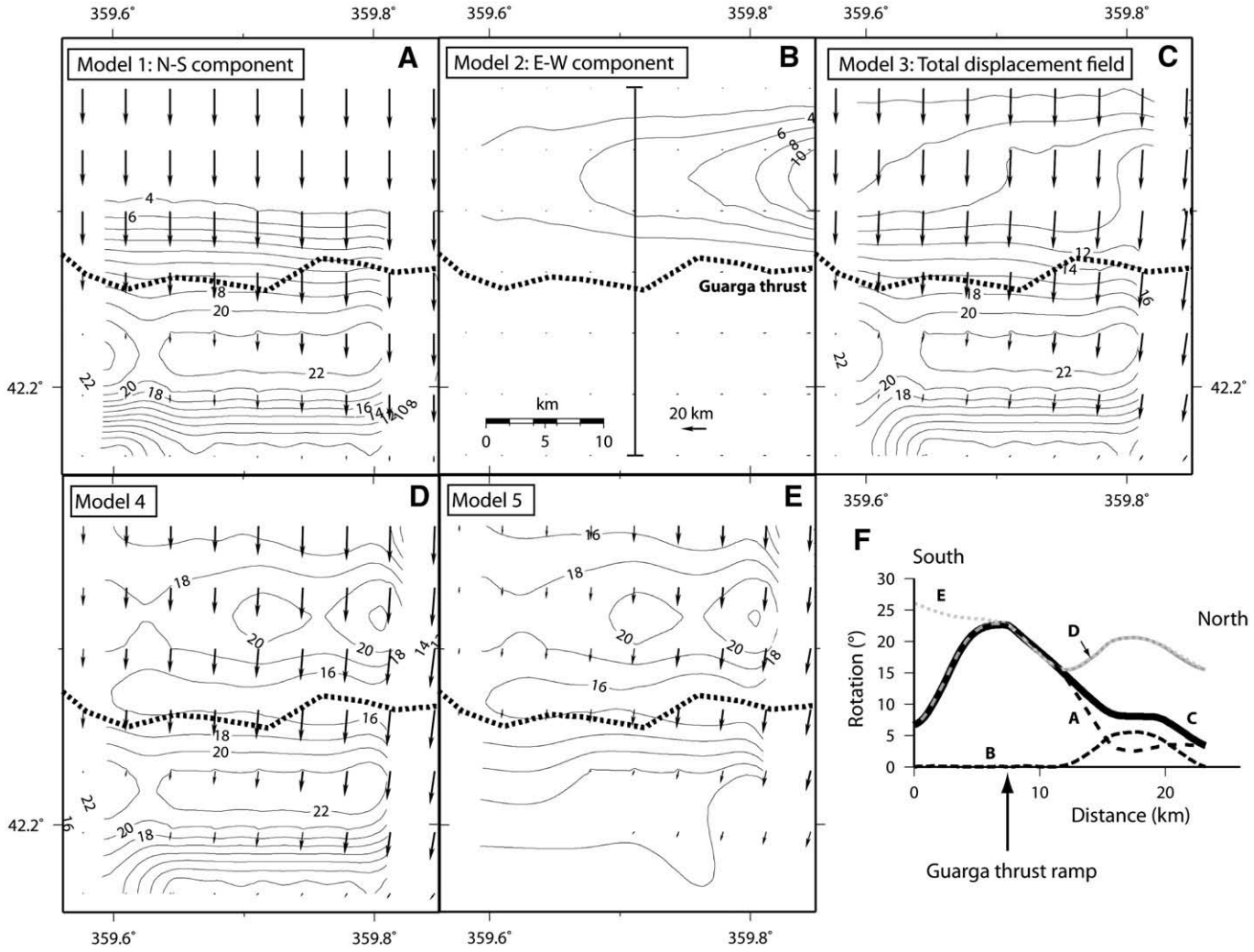

Fig. 6. Finite vertical-axis rotations predicted in the hangingwall and footwall of the Upper Guarga thrust (black dashed line) as a function of the different components of N–S and E–W finite displacements. All rotations shown as labeled contour lines are positive meaning that they are all clockwise. A) Model 1; rotations (labeled contour lines) predicted by the distribution of the N–S component of displacement shown as black arrows. B) Model 2: Same as A, but for the E–W component. C) Model 3: finite rotations predicted by combined N–S and E–W components of total horizontal displacement field. D) Model 4: rotations predicted after the partial restoration of the out-of-sequence Upper Guarga thrust sheet units (see text for explanations). E) Model 5: rotations predicted by the partial restoration of 10-km taken up by the N–S translation along the Lower Guarga thrust. F) Distance–rotation profiles obtained for models presented above. Location of the studied section is presented in B.

Table 1
Summary of the kinematic models shown in Fig. 7.

Model	Rotation		Time interval (Ma, mean)	Mean shortening (km)	Shortening rates (km/Ma)
	Footwall	Hangingwall			
1	14.2° ± 2.3° (22.3°)	3.1° ± 0.4° (4.7°)	–	–	–
2	0	4.8° ± 1.1° (10.1°)	–	–	–
3	14.6° ± 2.4° (22.3°)	6.5° ± 1° (10.7°)	[30–16] (23)	9.5 ± 2.6	0.39 ± 0.27
4	14.6° ± 2.4° (22.3°)	16.6° ± 1.5° (20.8°)	[37–30] (33.5)	10	3.3
5	17.4° ± 3.7° (33.2°)	16.5° ± 1.5° (20.8°)	[41.2–37] (39.1)	13 ± 3.6	3.09 ± 0.27

We also indicate the mean finite rotations with 95% confidence intervals for each model of restoration including in parentheses the maximum rotation calculated.

hangingwall of the Lower Guarga thrust (Fig. 7). The remaining displacement field illustrated in Model 5 (Fig. 6E) corresponds to the initial displacement gradient responsible for the rotations of ~20° observed within the syntectonic strata of Bartonian and Early Priabonian age (Pueyo et al., 2002). We finally predict an average shortening of 13 ± 3.6 km associated with a clockwise rotation of 16.6° ± 1.5° in agreement with these observations.

4.3. Discrepancies between predicted and observed rigid rotations

We were successful in reproducing the intermediate Bartonian rotations of about 20° reported regionally within the Jaca basin (Oliva-Urcia and Pueyo, 2007) and the rotations of 21.1° ± 8.8° measured within the Bartonian deposits of the Arguis syncline (Fig. 1) (Pueyo et al., 2002). However, the predicted finite rotation of 10.7° in the hangingwall of the Upper Guarga thrust unit is explained by a secondary counterclockwise rotation. As a difference of 10° implies an error of the order of 9 km on the displacement gradient this result deserves more explanations. The error could first arise from the inaccuracy in the geological cross-sections, especially on the proposed geometry of the out-of-sequence Upper Guarga thrust ramp. This explanation is however untenable considering the scale of the studied area, which is only 25 × 25 km. One proposes that the second rotation, which is thought to be Late Oligocene–Early Miocene was not recorded by the sediment

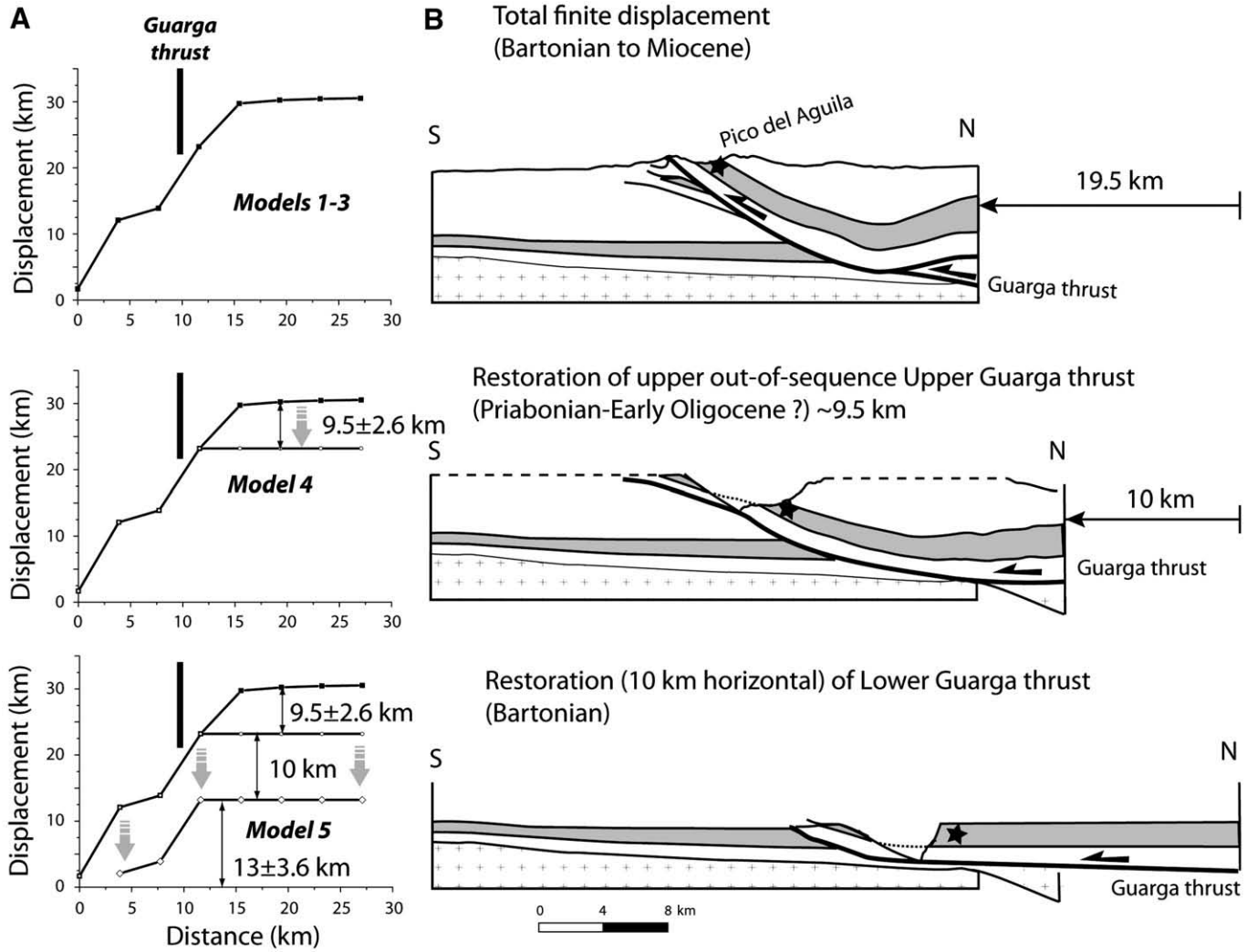

Fig. 7. Longitudinal profiles of displacement (N–S component) as a function of the successive restoration of the Upper and Lower Guarga thrust sheets according to Models 1–5 in Fig. 6. A) Longitudinal profiles of the position of grid nodes represented as black arrows in Figs. 5 and 6 as a function of their displacements (N–S component). B) Sketch of the restored cross-section AA′ (Fig. 3) at the longitude of the Pico del Aguila anticline. The black star tracks the position of the Pico del Aguila anticline at each restoration step.

grains (mainly Bartonian in age) in which paleomagnetic rotations have been obtained. A first possible reason would be related to internal deformation recorded by those Eocene sediments during the out-of-sequence Upper Guarga thrusting. By cutting through the whole sedimentary cover, this thrust probably produced noticeable changes in the stress state and caused locally strong deformation and damage in the hangingwall. For instance, the development of oblique strike-slip faulting in the hangingwall would have been able to accommodate the differential shortening through distributed strike-slip displacements without any vertical-axis rotation as it was proposed in other similar structural settings (e.g., Mouthereau et al., 1999). Such a local tectonic shear would be responsible for overestimating the finite regional rotations. A second source of error can be related to the spurious vertical-axis rotation caused by the superimposition of two non-coaxial horizontal direction of shortening at the intersection of oblique and frontal ramps. Given the above issues on the interpretation of paleomagnetic rotations, we hence conclude that our predictions are correct and can be used to investigate the sequence of shortening.

5. The propagation of the southern Pyrenean tectonic wedge in the Middle–Late Paleogene–Early Neogene

5.1. Sequence of deformation from 41 Ma to 16 Ma

We have established that the Jaca basin and the Sierras Exteriores underwent a mean clockwise rotation of 16.5° ± 1.5° (Fig. 8 and Table 1) during the Bartonian, i.e., between 41 Ma and 37 Ma. This result is consistent with the paleomagnetic rotations estimated in the same area (Oliva-Urcia and Pueyo, 2007). Such a rotation was achieved in relation with the southward transport of the Lower Guarga thrust sheet and a mean shortening of 13 ± 3.6 km (Model 5 of Figs. 6E and 7). The numerous sedimentological studies of the Eocene deposits show that the Jaca wedge-top basin and the associated feeding system established on top of the Lower Guarga thrust (Fig. 9). The catchments that delivered the synorogenic sediments into the Jaca basin were principally located on top of the exhumed Boltaña–Gavarnie thrust unit in the central and eastern Pyrenees and in the North of the Jaca basin (Fig. 9). The coeval tectonic activity of the Boltaña anticline (Fig. 2) suggests that the Gavarnie–Boltaña thick-skinned unit, to the rear, and the Lower Guarga thin-skinned unit, to the front, were both genetically connected. Zircon and apatite fission-track ages obtained in the Gavarnie thrust (Neouvielle Massif and Marimana Massif) confirm that its activity dates back to ~50 Ma and might have been continuous until ~32 Ma (Sinclair et al., 2005; Jolivet et al., 2007). The mean rate of shortening is consequently 3.09 ± 0.27 km/Ma (Table 1). The second phase of deformation started between 37 and 30 Ma during the Priabonian–Oligocene. According to our kinematic reconstructions, this episode is characterized by a translation of 10 km taken up by thin-skinned deformation above the Trias basal décollement. This occurs with slightly higher rates of displacement of 3.3 km/Ma. However, the difference is probably not significant since error bars on stratigraphic ages are large. In the internal domain, fission-track ages suggest that the southward translation was associated with the exhumation of the Gavarnie unit until ~32 Ma (Sinclair et al., 2005; Jolivet et al., 2007). As it will be discussed in the next section, this phase of exhumation might also be the result of enhanced erosion. The third phase finally occurred in the Late Oligocene–Early Miocene, between 30 and 16 Ma, when the out-of-sequence Upper Guarga thrust ramp activated. This episode was characterized by a shortening of 9.5 ± 2.6 km. The large time interval considered and the age uncertainties lead to propose rates of shortening of 0.39 ± 0.27 km/Ma. During this period, the hangingwall of the Upper Guarga ramp recorded a counterclockwise rotation so as to finally preserve the 10.7° of clockwise rotation (Fig. 8 and Table 1). This episode of thrusting in the sediment cover is associated with the initiation of the Guarga basement thrust, which is responsible for the development of the rio Guarga syncline.

5.2. Pyrenean pro-wedge propagation rates and orogenic fluxes

In order to provide a valuable interpretation of our reconstructed shortening rates at the scale of the pro-wedge of the Pyrenees, we compare, in the following, the rates of shortening obtained in this study with those estimated at other localities of the southern thrust front of the Pyrenees. Based on our kinematic model, we have constrained rates of shortening of ~3 km/Ma for the period ranging between 41.2 and 30 Ma (Fig. 8B). This result is close to the rates of shortening reconstructed using geometric relationships between synorogenic strata and thrusting. For instance, Vergés et al. (2002) proposed rates of 1.5 to 2.6 km/Ma in the Eastern Pyrenees during approximately the same period and Meigs et al. (1996) estimated consistent rates of shortening of 2.36 km/Ma between 37 and 24.7 Ma across the Sierras Marginales in the Central Pyrenees. We hence infer that, on the pro-wedge side of the orogen, the material was accreted at nearly the same rate from East to West during the period comprised between the Bartonian and the Middle Oligocene.

Based on those estimates at the thrust front, we can try to examine further the possible changes in mass balance within the Pyrenean tectonic wedge from the Bartonian to the Middle Oligocene. Our approach here does not intend at providing accurate estimates of the fluxes, especially the erosion fluxes, which cannot currently be done given the data available in the literature and in this work. Instead, we seek to provide a first-order evaluation of the evolution of incoming and outcoming fluxes within the pro-Pyrenean wedge in association with the thickening of the Iberian crust. However, since we use constraints on thermo-chronometric ages, our results show significant improvements with respect to previous estimates on erosion fluxes that were obtained by equating erosion to rock uplift from restored crustal-scale cross sections in the eastern (Vergés et al., 1995) and west-central Pyrenees (Teixell, 1998).

We assume that the accreted material is entering the wedge at the pro-wedge side of the orogenic wedge. This approximation is justified by the fact that the horizontal shortening on the retro-wedge, i.e. in the Northern Pyrenees, was limited during the Tertiary and has ceased by the end of the Bartonian (Sinclair et al., 2005).

During the period ranging from 41 Ma to 37 Ma, we have established that the pro-wedge widened by accretion above a décollement located in the Trias evaporites. Shortening occurred by accretion of the Lower Guarga thrust at a rate of 3.09 ± 0.27 km/Ma, within the sediment cover (Table 1 and Fig. 8), and by sliding northwards along the Gavarnie–Boltaña basement thrust, which was initiated earlier in the Lutetian (Fig. 2). According to Fig. 3 (e.g. see section AA′) a thickness of 5 km for the newly accreted material is adopted. We thus obtain incoming accretionary fluxes of ~15 km^2/Ma on the pro-wedge side of the orogen.

Outcoming fluxes are constrained by available apatite fission-track (AFT) ages-altitudes profiles (Fitzgerald et al., 1999) and by multiple AFT dating and (U–Th)He dating on apatite grains (Gibson et al., 2007) in the Central Pyrenees. Fitzgerald et al. (1999) indicated low rates of denudation of 0.173 km/Ma for the period 50–35 Ma in the Riberot Massif of the Gavarnie unit, and Gibson et al. (2007) estimated comparable denudation rates of 0.3 km/Ma in the Maladeta Massif of the Guarga–Orri unit, but for a longer period comprised between 50 Ma and 31 Ma.

The eroded width of the orogen is a major unknown to the quantification of erosion fluxes during the Bartonian. The paleogeography of the Bartonian sediments suggests that the Axial Zone was a topographic ridge, large enough to enable the development of a large river network feeding the foreland basin (Fig. 9). Moreover, given the thrust front displacement of 27 km (Fig. 4) and a partially restored crustal-scale cross-section (Teixell, 1998) we finally estimate that the

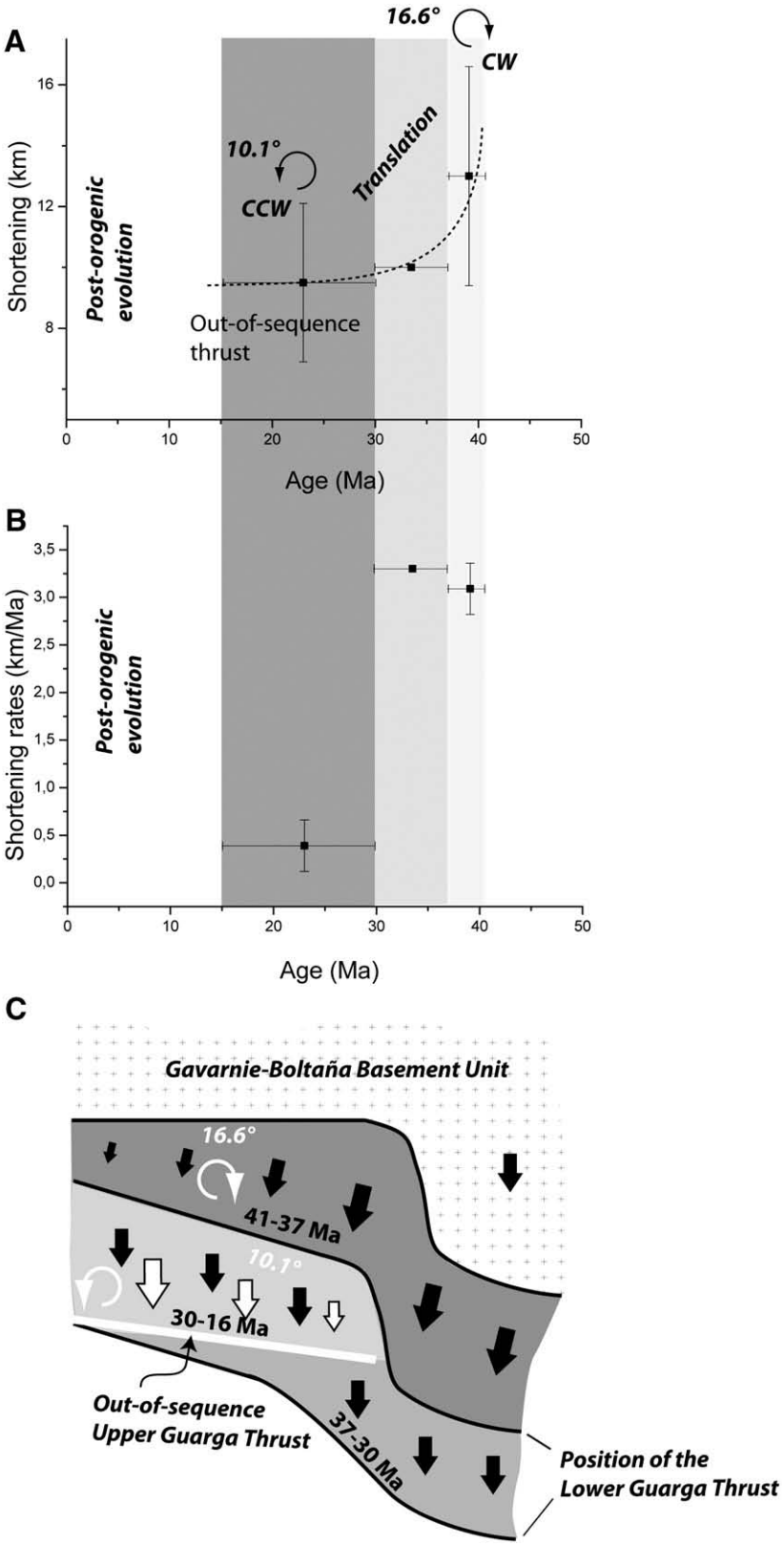

Fig. 8. Plots of mean shortening A) and mean rates of shortening B) through time. Abbreviations: CW for clockwise rotation and CCW for counter-clockwise rotation. C) shows the schematic reconstruction of the deformation patterns (rotations, translation) including the position of the Lower and the Upper Guarga thrust sheet for each time step at ~39.1 Ma, ~33.5 Ma and ~23 Ma which is also outlined by different grey-shaded colors (lighter means younger). Note that the last increment of shortening is related to out-of-sequence emplacement of the Upper Guarga thrust sheet.

exhumed domain could not be larger than 50 km during the Bartonian. Given a width for the wedge of 50 km and by extrapolating the denudation rates, we obtain outcoming fluxes of 11.6 ± 6.2 km^2/Ma (Fig. 10). Frontal accretionary fluxes and outcoming fluxes show comparable values, which suggests a dynamic equilibrium within the Pyrenean wedge during the Bartonian.

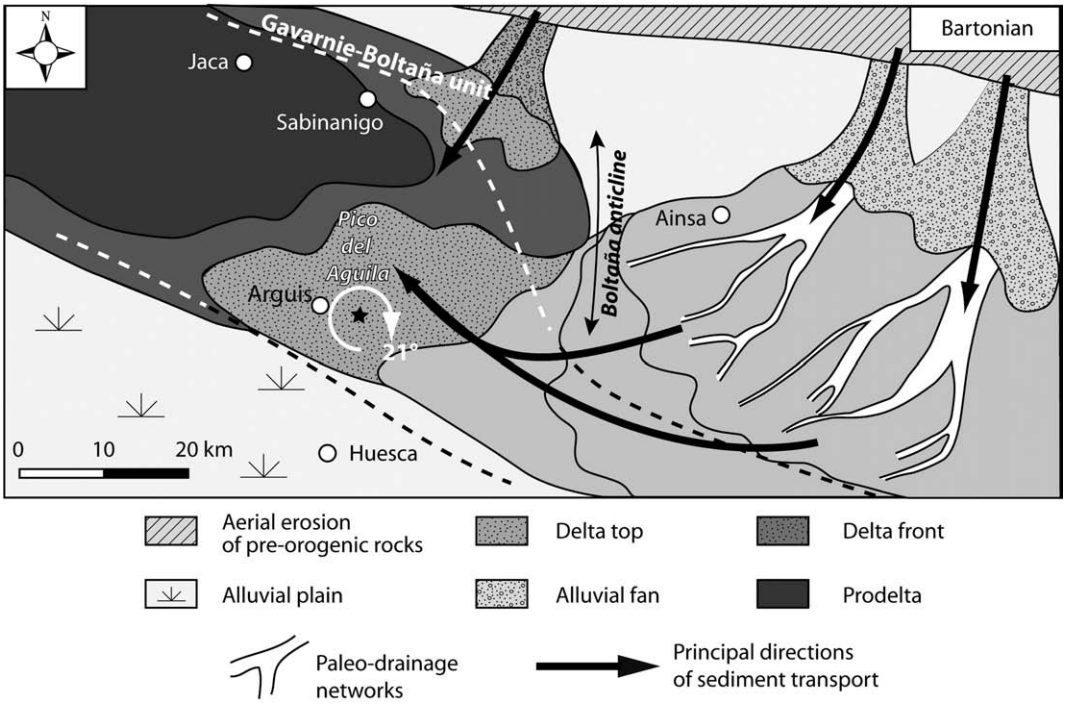

Fig. 9. Paleogeographic and tectonic reconstruction during the Bartonian based on a compilation of available reconstructions (Plaziat, 1981; Nijman, 1998; Dreyer et al., 1999) and maps (Millán Garrido, 1996). Rotations coeval with the growth of the Pico del Aguila anticline are related to the particular distribution of shortening associated with the propagation of the southern thrust front produced by the foreland migration of the Gavarnie–Boltaña basement thrust unit. Dashed lines outline the possible position of the main thrust faults in relation with the Gavarnie–Boltaña unit and the southern thrust front.

Between 37 Ma and 30 Ma, we estimate nearly equivalent displacement rates of 3.3 km/Ma. However, the lack of newly accreted thrust unit suggests that the pro-wedge widened by stable sliding along the Lower Guarga thrust at this time (Figs. 7 and 8). Northwards, the displacement is taken up by sliding along the Gavarnie–Boltaña basement unit in agreement with tectonic reconstruction (Teixell, 1996). We hence infer a lack of frontal accretionary flux at this time.

In contrast, thermochronometric constraints suggest a rapid increase of cooling rates in the hinterland of the Central Pyrenees of 2–4 km/Ma in the Maladeta massif of the Guarga–Orri unit between 35 and 30 Ma (Fitzgerald et al., 1999) consistent with denudation rates of 1–1.5 km/Ma between 31 and 29 Ma proposed by Gibson et al. (2007) in the same unit. If we assume a conservative eroded width of 50 km and a mean denudation rate of 3 ± 1.7 km/Ma, the flux of material eroded from the orogen is estimated to be up to ~150 km^2/Ma (Fig. 10). Such a value is however probably overestimated since we refer to a local denudation rate and because cooling rates are expected to decrease laterally N–S across the Pyrenean orogen. For comparison, a double-sided wedge of 50 km (such as presented in Fig. 10) with maximum denudation rates of 3 ± 1.7 km/Ma at the wedge center, and rates decreasing to zero at wedge toes, would give a minimum outcoming fluxes of ~75 km^2/Ma.

To explain the excess of denudation flux with respect to frontal accretionary flux, one can hypothesize the acceleration of tectonics through underplating, enhanced erosion due to climate changes or a combination of both in order to maintain the mass balance within the pro-wedge.

Underplating below the Guarga–Orri unit, for instance, by the Rialp unit in eastern Pyrenees (e.g. Muñoz, 1992), has been proposed as a possible mechanism for accretion in order to balance the observed acceleration of denudation in the Maladeta massif (Sinclair et al., 2005). However, after the collision started in the late Cretaceous, the Iberia/Eurasia plate convergence declined during the Paleogene as supported by the decrease of shortening rates. As a consequence, the acceleration of accretionary flux through underplating is not consistent with the expected decrease of plate convergence. Moreover, assuming that accretion was dominated by underplating, the flux accreted from below the wedge would be maximum 30 km^2/Ma, during the interval 37–30 Ma (Fig. 10). This amount is still 2.5 to 5 times lower than the observed outcoming fluxes. Moreover, the Oligocene was characterized by the backfilling of the southern Pyrenean fold-thrust belt up to the Axial Zone with the accumulation of several kilometers of continental conglomerates (e.g. Coney et al., 1996; Babault et al., 2005), which seems hardly compatible with rapid tectonic uplift in the hinterland.

If tectonics, through underplating, is not the unique cause for increased denudation, one has to consider climate as a possible relevant forcing mechanism. The Eocene–Oligocene climatic transition, occurring at ~34 Ma, is one of the largest global cooling events of the Tertiary (Katz et al., 2008), characterized in particular by the establishment of large permanent Antarctic ice sheets (Coxall et al., 2005; Lear et al., 2008) attested by the fall of global sea-level (Miller et al., 2005). There are many evidences of a coupling between this climatic shift, the seasonal gradient of temperature and the increase of global erosion (e.g. Zachos et al., 1999; Ivany et al., 2000; Eldrett et al., 2009). We suggest that such a major cooling event at the Eocene–Oligocene transition (Zachos et al., 2001) can explain the rapid denudation, backfilling and the absence of comparable accretion.

Since 30 Ma, we have reported a decrease of the rates of shortening at the front to 0.39 ± 0.27 km/Ma in the Late Oligocene–Early Miocene (Table 1 and Fig. 8). Such a decrease is coeval, in our study area, with the imbrication of the Guarga–Orri basement unit in front of the Gavarnie–Boltaña basement unit, which leads to increase the thickness of material accreted to the Pyrenean orogen (Fig. 10). Considering a higher accreted thickness of 15 km, we deduce accretionary fluxes of 5.85 km^2/Ma consistent with the reduction of plate convergence. The few constraints on the exhumation rates give 0.03 km/Ma from the Maladeta massif of the Guarga–Orri unit which reveal tectonic and thermal stability between 30 and 20 Ma (Fitzgerald et al., 1999). Taking into account an exhumation window

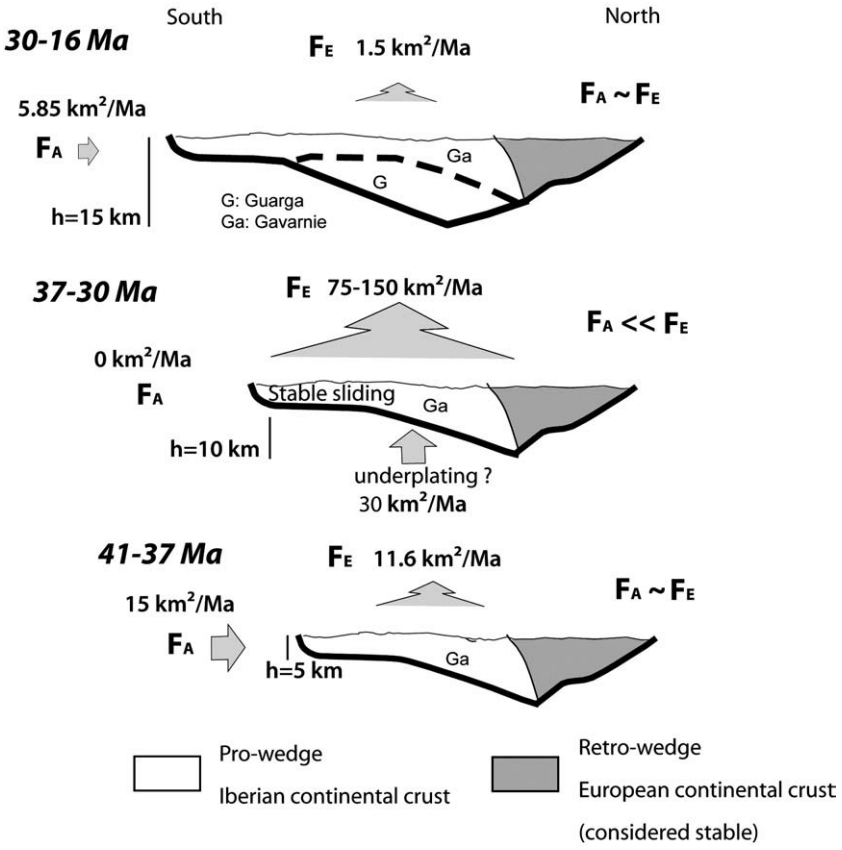

Fig. 10. Evolution of accretionary (FA) and erosion (FE) fluxes in the southern Pyrenean thrust wedge since 41 Ma. The large exhumation flux at 37–30 Ma is interpreted as the consequence of enhanced erosion due to global cooling. At this time, the Pyrenean pro-wedge widens by stable sliding along the Lower Guarga thrust. To estimate the potential occurrence of underplating at this time, we have considered thickness *h* of material entering the wedge below the Trias décollement that is 10 km times the displacement rate of ~3 km/Ma reconstructed from this study (Fig. 8). The minimum outcoming flux of 75 km^2/Ma has been estimated by taking into account lateral variations of denudation rates and the maximum flux of 150 km^2/Ma is based on uniform denudation rates distribution (see text for explanation). After 30 Ma, the rate of wedge widening is significantly reduced. The accreted thicknesses *h* increase between steps 41–37 Ma and 30–16 Ma due to the frontal imbrication of the Guarga basement unit.

of 50 km we deduce a maximum denudation flux of 1.5 km^2/Ma in agreement with the overall evolution towards steady post-orogenic fluxes (Fig. 10).

The cumulated eroded area between 41 and 16 Ma can be roughly estimated to be maximum 1117 km^2 based on our study. This is about twice the eroded fluxes proposed from fully restored crustal-scale cross sections, e.g. 580 km^2 for Vergés et al. (1995) and 575 km^2 for Teixell (1998). Teixell (1998) also calculated that a cross-sectional area of ~900 km^2 was deposited in the Ebro foreland basin during the Tertiary. The excess foreland sedimentation was previously interpreted to be related to sediment sourced from the east, out of the studied cross section. Since the estimates presented in this study accounts for published denudation rates they show eroded area that is also more consistent with the depositional area observed in the Ebro foreland.

6. Conclusions

The approach adopted in this study, based on the reconstruction of the finite strains and finite rotations, provides new constraints on the Cenozoic propagation of the southern Pyrenean front and on the evolution of the Pyrenean wedge.

We distinguish three main episodes of shortening between 41 and 37 Ma, 37 and 30 Ma and between 30 and 16 Ma. The first period coincides with the development of the Boltaña–Gavarnie basement unit coeval with the southward propagation of cover thrust sheets above the Trias décollement. A mean rotation of $16.6° \pm 1.5°$ is predicted by the distribution of both E–W and N–S components of shortening within the Guarga cover units. Such rotations are in agreement with measured paleomagnetic rotations of $21.1° \pm 8.8°$ (Pueyo et al., 2002). The second period is interpreted to be dominated by a southward translation of 10 km of the thrust front, the basal cover décollement rooted at depth into the Gavarnie basement thrust. Our study thus brings new constraints for this specific time interval which lacks field evidence of syntectonic sedimentary records. During the third episode, the frontal accretion of the Guarga basement thrust in front of the Gavarnie thrust is associated with the development of the rio Guarga syncline and the emergence of the Sierras Exteriores along the out-of-sequence Upper Guarga thrust ramp. The overall decrease of the accretionary rates from ~3 km/Ma to 0.39 ± 0.27 km/Ma is well in agreement with the consumption of Iberia plate convergence relative to Eurasia from the Middle Eocene to Oligo-Miocene times. The period between 37 and 30 Ma exhibits large outcoming fluxes estimated of maximum 150 km^2/Ma that are not fully compensated by accretionary fluxes within the Pyrenean wedge. There are several lines of evidence suggesting that such a strong decoupling between incoming and outcoming fluxes can be related to climate-induced erosion during the abrupt cooling recorded at the Eocene–Oligocene boundary.

Acknowledgements

The authors would like to thank N. Bellahsen for discussions about the tectonics of the Pico del Aguila anticline during several field surveys. A special thank goes to J. Serra-Kiel from the Barcelona University for his help in the field and discussions. The French CNRS has provided partial funding for this research. Thoughtful comments

by two anonymous reviewers helped to improve the original version of the manuscript.

Appendix A. Supplementary data

Supplementary data associated with this article can be found, in the online version, at doi:10.1016/j.epsl.2009.10.002.

References

Babault, J., Van den Driessche, J., Bonnet, S., Castelltort, S., Crave, A., 2005. Origin of the highly elevated Pyrenean peneplain. Tectonics 24. doi:10.1029/2004TC001697.

Castelltort, S., Guillocheau, F., Robin, C., Rouby, D., Nalpas, T., Lafont, F., Eschard, R., 2003. Fold control on the stratigraphic record: a quantified sequence stratigraphic study of the Pico del Aguila anticline in the south-western Pyrenees (Spain). Basin Res. 15, 527–551. doi:10.1046/j.1365-2117.2003.00218.x.

Coney, P.J., Muñoz, J.A., McClay, K.R., Evenchick, C.A., 1996. Syntectonic burial and post-tectonic exhumation of the southern Pyrenees foreland fold-thrust belt. J. Geol. Soc. 153, 9–16.

Coxall, H.K., Wilson, P.A., Palike, H., Lear, C.H., Backman, J., 2005. Rapid stepwise onset of Antarctic glaciation and deeper calcite compensation in the Pacific Ocean. Nature 433, 53–57.

Dinarès, J., McClelland, E., Santanach, P., 1992. Contrasting rotations within thrust sheets and kinematics of thrust tectonics as derived from paleomagnetic data: an example from the southern Pyrenees. In: McClay, K.R. (Ed.), Thrust Tectonics. Chapman & Hall, London, pp. 265–275.

Dreyer, T., Corregidor, J., Arbues, P., Puigdefàbregas, C., 1999. Architecture of the tectonically influenced Sobrarbe deltaic complex in the Ainsa Basin, northern Spain. Sed. Geol. 127, 127–169.

Eldrett, J.S., Greenwood, D.R., Harding, I.C., Huber, M., 2009. Increased seasonality through the Eocene to Oligocene transition in northern high latitudes. Nature 459, 969–974.

Fernàndez, O., Muñoz, J.A., Arbues, P., Falivene, O., Marzo, M., 2004. Three-dimensional reconstruction of geological surfaces: an example of growth strata and turbidite systems from the Ainsa basin (Pyrenees, Spain). AAPG Bulletin 88, 1049–1068.

Fitzgerald, P.G., Muñoz, J.A., Coney, P.J., Baldwin, S.L., 1999. Asymmetric exhumation across the Pyrenean orogen: implications for the tectonic evolution of a collisional orogen. Earth Planet. Sci. Lett. 173, 157–170.

Gibson, M., Sinclair, H.D., Lynn, G.J., Stuart, F.M., 2007. Late- to post-orogenic exhumation of the Central Pyrenees revealed through combined thermochronological data and modelling. Basin Res. 19, 323–334.

Hirst, J.P.P., Nichols, G.J., 1986. Thrust tectonic controls on alluvial sedimentation patterns, southern Pyrenees. In: Allen, P.A., Homewood, P. (Eds.), Foreland Basins 8 Spec. Publ. Int. Ass. Sediment, pp. 247–258.

Hogan, P.J., Burbank, D.W., 1996. Evolution of the Jaca piggyback basin and emergence of the External Sierras, southern Pyrenees. In: Friend, P., Dabrio, C. (Eds.), Tertiary Basins of Spain: the Stratigraphic Record of Crustal Kinematics 6. Cambridge University Press, Cambridge, pp. 153–160.

Holl, J.E., Anastasio, D.J., 1993. Paleomagnetically derived folding rates, southern Pyrenees, Spain. Geology 21, 271–274.

Ivany, L.C., Patterson, W.P., Lohmann, K.C., 2000. Cooler winters as a possible cause of mass extinctions at the Eocene/Oligocene boundary. Nature 407, 887–890.

Jolivet, M., Labaume, P., Monie, P., Brunel, M., Arnaud, N., Campani, M., 2007. Thermochronology constraints for the propagation sequence of the south Pyrenean basement thrust system (France–Spain). Tectonics 26. doi:10.1029/2006TC002080.

Katz, M.E., Miller, K.G., Wright, J.D., Wade, B.S., Browning, J.V., Cramer, B.S., Rosenthal, Y., 2008. Stepwise transition from the Eocene greenhouse to the Oligocene icehouse. Nature Geosciences 1, 329–334.

Lear, C.H., Bailey, T.R., Pearson, P.N., Coxall, H.K., Rosenthal, Y., 2008. Cooling and ice growth across the Eocene–Oligocene transition. Geology 36, 251–254.

McCaig, A.M., McClelland, E., 1992. Palaeomagnetic techniques applied to thrust belts. In: McClay, K.R. (Ed.), Thrust Tectonics. Chapman & Hall, London, pp. 209–216.

Meigs, A., Vergés, J., Burbank, D.W., 1996. Ten-million-year history of a thrust sheet. Geol. Soc. Am. Bull. 108, 1608–1625.

Meigs, A.J., Burbank, D.W., 1997. Growth of the South Pyrenean orogenic wedge. Tectonics 16, 239–258.

Millán Garrido, H., 1996. Estructura y cinematica del frente de cabalgamiento surpirenaico en las Sierras Exteriores Aragonesas. Universidad de Zaragoza.

Millán, H., Aurell, M., Melendez, A., 1994. Synchronous detachment folds and coeval sedimentation in the Prepyrenean External Sierras (Spain): a case study for a tectonic origin of sequences and systems tracts. Sedimentology 41, 1001–1024.

Miller, K.G., Kominz, M.A., Browning, J.V., Wright, J.D., Mountain, G.S., Katz, M.E., Sugarman, P.J., Cramer, B.S., Christie-Blick, N., Pekar, S.F., 2005. The phanerozoic record of global sea-level change. Science 310, 1293–1298.

Morris, R.G., Sinclair, H.D., Yelland, A.J., 1998. Exhumation of the Pyrenean orogen: implications for sediment discharge. Basin Res. 10, 69–85.

Mouthereau, F., Lacombe, O., Deffontaines, B., Angelier, J., Chu, H.-T., Lee, C.-T., 1999. Quaternary transfer faulting and belt front deformation at Pakuashan (western Taiwan). Tectonics 18, 215–230.

Muñoz, J.A.E., 1992. Evolution of a continental collision belt: ECORS-Pyrenees crustal balanced cross-section. In: McClay, K. (Ed.), Thrust Tectonics. Chapman & Hall, pp. 235–246.

Nijman, W., 1998. Cyclicity and basin axis shift in a piggy-back basin: towards modelling of the Eocene Tremp–Ager Basin, South Pyrenees, Spain. In: Mascle, A., Puigdefàbregas, C., Luterbacher, H.P., Fernández, M. (Eds.), Cenozoic Foreland Basins of Western Europe, 134. Geol. Soc. Spec. Publ, pp. 135–162.

Oliva-Urcia, B., Pueyo, E.L., 2007. Gradient of shortening and vertical-axis rotations in the southern Pyrenees (Spain), insights from a synthesis of paleomagnetic data. Revista de la Sociedad Geológica de España, vol. 20, pp. 105–118.

Plaziat, J.-C., 1981. Late Cretaceous to Late Eocene palaeogeographic evolution of southwest Europe. Palaeogeogr. Palaeoclimatol. Palaeoecol. 36, 236–320.

Poblet, J., Hardy, S., 1995. Reverse modelling of detachment folds; application to the Pico del Aguila anticline in the South Central Pyrenees (Spain). J. Struct. Geol. 17, 1707–1724.

Pueyo, E.L., Millàn, H., Pocoví, A., 2002. Rotation velocity of a thrust: a paleomagnetic study in the External Sierras (Southern Pyrenees). Sed. Geol. 142, 191–208.

Pueyo, E.L., Parés, J.M., Millán, H., Pocoví, A., 2003. Conical folds and apparent rotations in paleomagnetism (a case studied in the Southern Pyrenees). Tectonophysics 362, 345–366.

Puigdefàbregas, C., Souquet, P., 1986. Tectono-sedimentary cycles and depositional sequences of the Mesozoic and Tertiary from the Pyrenees. Tectonophysics 129, 173–203.

Sinclair, H.D., Gibson, M., Naylor, M., Morris, R.G., 2005. Asymmetric growth of the Pyrenees revealed through measurement and modeling of orogenic fluxes. Am. J. Sci. 305, 369–406.

Teixell, A., 1996. The Anso transect of the southern Pyrenees: basement and cover thrust geometries. J. Geol. Soc. 153, 301–310.

Teixell, A., 1998. Crustal structure and orogenic material budget in the west central Pyrenees. Tectonics 17, 395–406.

Vergés, J., Millán, H., Muñoz, J.A., Marzo, M., Cirès, J., Den Bezemer, T., Zoetemeijer, R., Cloetingh, S., 1995. Eastern Pyrenees and related foreland basins: pre-, syn- and post-collisional crustal-scale cross-sections. Mar. Petrol. Geol. 12, 893–915.

Vergés, J., Fernàndez, M., Martínez, A., 2002. The Pyrenean orogen: pre-, syn-, and post-collisional evolution. In: Rosenbaum, G., Lister, G. (Eds.), Reconstruction of the evolution of the Alpine–Himalayan Orogen, 8, pp. 55–74.

Zachos, J.C., Opdyke, B.N., Quinn, T.M., Jones, C.E., Halliday, A.N., 1999. Early Cenozoic glaciation, Antarctic weathering, and seawater $^{87}Sr/^{86}Sr$: is there a link? Chem. Geol. 161.

Zachos, J., Pagani, M., Sloan, L., Thomas, E., Billups, K., 2001. Trends, rhythms, and aberrations in global climate 65 Ma to present. Science 292, 686–693.